PHYSICAL REVIEW B **92**, 020508(R) (2015)

Tunable electronic anisotropy in single-crystal $A_2Cr_3As_3$ (A=K, Rb) quasi-one-dimensional superconductors

X. F. Wang,[1] C. Roncaioli,[1] C. Eckberg,[1] H. Kim,[1] J. Yong,[1] Y. Nakajima,[1] S. R. Saha,[1] P. Y. Zavalij,[2] and J. Paglione[1,3]
[1]*Center for Nanophysics and Advanced Materials, Department of Physics, University of Maryland, College Park, Maryland 20742, USA*
[2]*Department of Chemistry, University of Maryland, College Park, Maryland 20742, USA*
[3]*Canadian Institute for Advanced Research, Toronto, Canada M5G 1Z8*
(Received 28 May 2015; published 20 July 2015)

Single crystals of $A_2Cr_3As_3$ (A = K, Rb) were successfully grown using a self-flux method and studied via structural, transport, and thermodynamic measurement techniques. The superconducting state properties between the two species are similar, with critical temperatures of 6.1 and 4.8 K in $K_2Cr_3As_3$ and $Rb_2Cr_3As_3$, respectively. However, the emergence of a strong normal state electronic anisotropy in $Rb_2Cr_3As_3$ suggests a unique electronic tuning parameter is coupled to the interchain spacing in the $A_2Cr_3As_3$ structure, which increases with alkali-metal ionic size while the one-dimensional $[(Cr_3As_3)^{2-}]_\infty$ chain structure itself remains essentially unchanged. Together with dramatic enhancements in both conductivity and magnetoresistance (MR), the appearance of a strong anisotropy in the MR of $Rb_2Cr_3As_3$ is consistent with the proposed quasi-one-dimensional character of band structure and its evolution with alkali-metal species in this new family of superconductors.

DOI: 10.1103/PhysRevB.92.020508 PACS number(s): 74.25.fc, 74.25.Ha, 74.25.Bt, 74.78.−w

The recent discovery of superconductivity in $A_2Cr_3As_3$ (A = K [1], Rb [2], and Cs [3]) has garnered significant attention due to the possible presence of reduced dimensionality in both normal and superconducting state properties. Superconductivity in quasi-one-dimensional (quasi-1D) systems presents a unique set of properties, including exotic deviations from expected behavior such as found in orbital magnetic field properties, as well as unconventional pairing in the form of singlet d-wave [4] and triplet p-wave [5] order parameters that emerge.

The crystal structure of $A_2Cr_3As_3$ indeed has one-dimensional elements, composed of double-walled subnanotube $[Cr_3As_3]_\infty$ chains separated by alkali-metal atoms in a hexagonal unit cell, as shown in Fig. 1. This chain crystal structure is quite similar to the well-known quasi-1D superconductors such as the Bechgaard salts [6,7], and purple bronzes $Li_{0.9}Mo_6O_{17}$ [8] and $Tl_2Mo_6Se_6$ [9]. The reported superconducting state properties show some indications of reduced dimensions, including a very large upper critical field H_{c2} that exceeds the Pauli limit [1,2,10], and provide some evidence for an unconventional pairing mechanism, as evidenced by power-law behavior in specific heat [2] and penetration depth measurements [11] on polycrystalline samples, as well as strong magnetic fluctuations in nuclear magnetic resonance [12] measurements. However, due to the difficulties in interpreting measured properties of polycrystalline samples with potential low-dimensional aspects, it is imperative that single-crystalline samples are studied. For instance, reports of an unusual linear temperature dependence of resistivity in polycrystalline samples of $K_2Cr_3As_3$ and $Rb_2Cr_3As_3$ [1,2] have been contradicted by a recent single-crystal study of $K_2Cr_3As_3$ [10], which also reports a relatively weak anisotropy of the amplitude of H_{c2} between fields applied parallel ($H_\parallel$) and perpendicular ($H_\perp$) to the needlelike crystal orientation,which is the (001) direction of the crystal structure, raising the question about the dimensionality of the electronic structure in the $A_2Cr_3As_3$ family.

Here we report the successful growth of both $K_2Cr_3As_3$ and $Rb_2Cr_3As_3$ single crystals and their normal and superconducting state properties based on structural, transport, magnetic, and thermodynamic measurements. Comparing normal state transport properties between $K_2Cr_3As_3$ and $Rb_2Cr_3As_3$ single-crystal samples reveals several key differences, including a large increase in the electrical conductivity in $Rb_2Cr_3As_3$ consistent with the proposed band structure evolution, as well as the emergence of a strong magnetoresistance magnitude and anisotropy in $Rb_2Cr_3As_3$ that we relate to a tunable reduced structural dimensionality that is controlled by the alkali-metal species in the $A_2Cr_3As_3$ system.

$K_2Cr_3As_3$ and $Rb_2Cr_3As_3$ single crystals were grown using a self-flux method as previously reported [1,10]. Pieces of K and Rb alkali metal (99.8%, Alfa Aesar) and chromium (99.999%, Alfa Aesar) were combined with arsenic powder (99.99%, Alfa Aesar) into an alumina crucible and sealed in a nitrogen glovebox using a stainless steel tube/Swagelok cap configuration [13]. Growths were heated up to 1000 °C and kept at this temperature for one day, followed by slow cooling down to 650 °C. The Swagelok enclosure was then re-opened in a glovebox, revealing many single crystals with shiny, silver coloring and a thin, long needlelike shape that extends along the crystallographic [001] axis. Crystals were mechanically removed from the crucibles and visually inspected for residual flux and crystalline quality. We note that $Rb_2Cr_3As_3$ crystals are much more reactive than $K_2Cr_3As_3$, resulting in larger uncertainties in sample mass determinations. Resistivity measurements were performed using the standard four-terminal configuration in a commercial cryostat system. Contacts were made in a glovebox using silver paint, followed by coating of samples with Apiezon N-grease to avoid air exposure. Magnetization measurements were taken using both a commercial superconducting quantum interference device magnetometer and vibrating sample magnetometer for $K_2Cr_3As_3$ and $Rb_2Cr_3As_3$ samples, respectively. A needlelike specimen of $Rb_2Cr_3As_3$ with approximate dimensions 0.01 mm × 0.03 mm × 0.39 mm was used for x-ray crystallographic analysis with intensity data measured using a Bruker APEX-II CCD system equipped with a graphite monochromator and a MoKa sealed tube (λ = 0.71073 Å),

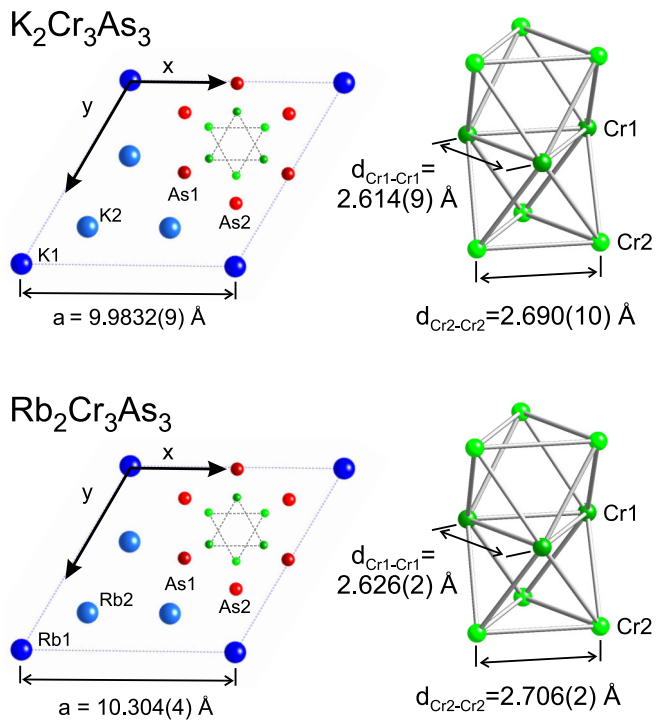

FIG. 1. (Color online) Schematic view of the structure of $K_2Cr_3As_3$ and $Rb_2Cr_3As_3$. A detailed comparison of the lattice parameters is listed in Table II. Data for $K_2Cr_3As_3$ is from Ref. [1].

with data collection performed at 90 and 250 K. The structure was solved and refined using the Bruker SHELXTL software package, using the space group $P\bar{6}m2$, with $Z = 2$ for the formula unit, $Rb_2Cr_3As_3$. The final anisotropic full-matrix least-squares refinement on $F2$ with 23 variables converged to $R1(w_{R2}) = 3.39\%$ (8.37%) and 3.85% (9.96%) at 90 and 250 K, respectively.

The lattice parameters of $Rb_2Cr_3As_3$ are larger than those of $K_2Cr_3As_3$, with the larger ionic radius of Rb (1.52 Å) as compared to K (1.38 Å) increasing the spacing between the $[Cr_3As_3]_\infty$ chains as shown in Fig. 1. Table I presents the atomic coordinates obtained from single-crystal x-ray analysis of $Rb_2Cr_3As_3$, with results well refined using a hexagonal crystal structure ($P\bar{6}m2$) and showing no symmetry changes when cooling down to 90 K. The unit cell of $Rb_2Cr_3As_3$ is 3.2% and 0.5% larger than that of $K_2Cr_3As_3$ [1] along the a- and c-axis directions, respectively. However, in contrast to the chain structure distortion previously reported for polycrystalline samples [1], the $[(Cr_3As_3)^{2-}]_\infty$ chain trunk width is almost identical for $Rb_2Cr_3As_3$ and $K_2Cr_3As_3$ as shown in Table II, displayed more clearly in Fig. 1. The Cr1-Cr1, Cr1-Cr2, and Cr2-Cr2 bond distances change less than 0.6% between $K_2Cr_3As_3$ and $Rb_2Cr_3As_3$, while the alkali-metal–arsenic bonds change by 3%–4%, consistent with a more simple expansion of the interchain distances with larger alkali-metal units and almost no influence on the chain structure itself. This presents a unique ability to tune the electronic density of a system while keeping the important structural elements unchanged, providing for an interesting "knob" to use for studying the emergence of reduced dimensional properties.

TABLE I. Atomic coordinates for $Rb_2Cr_3As_3$ single crystal, measured at 250 K.

Atom	Label	x	y	z	Wyckoff position	U_{eq}
Rb	Rb1	0.0	0.0	0.0	$3j$	0.0279(10)
Rb	Rb2	0.79519(14)	0.5904(3)	0.5	$3k$	0.0232(5)
Cr	Cr1	0.4183(2)	0.8366(4)	0.5	$3k$	0.0115(7)
Cr	Cr2	0.5084(5)	0.7542(2)	0.0	$3j$	0.0122(7)
As	As1	0.49505(14)	0.9901(3)	0.0	$1c$	0.0125(5)
As	As2	0.6581(3)	0.82907(15)	0.5	$3k$	0.0124(5)

TABLE II. Comparison of crystallographic data for $K_2Cr_3As_3$ (300 K) [1] and $Rb_2Cr_3As_3$ (250 and 90 K).

	$K_2Cr_3As_3$ [1] (300 K)	$Rb_2Cr_3As_3$ (250 K)	$Rb_2Cr_3As_3$ (90 K)
Space group	$P\bar{6}m2$	$P\bar{6}m2$	$P\bar{6}m2$
a (Å)	9.9832(9)	10.304(4)	10.251(5)
c (Å)	4.2304(4)	4.2514(18)	4.227(2)
V (Å^3)	365.13(6)	390.9(4)	384.7(4)
Bond distance	(A = K and Rb)		
A1-As1 (Å)	3.366(2)	3.484(2)	3.462(2)
A1-As2 (Å)	3.263(5)	3.393(2)	3.375(2)
A2-As1 (Å)	4.9916(13)	5.153(2)	5.126(2)
A2-As2 (Å)	3.562(3)	3.718(2)	3.693(2)
Cr1-As1 (Å)	2.516(4)	2.529(2)	2.516(2)
Cr1-As2 (Å)	2.510(3)	2.511(2)	2.504(2)
Cr2-As1 (Å)	2.490(3)	2.502(2)	2.494(2)
Cr2-As2 (Å)	2.506(4)	2.511(2)	2.497(2)
Cr1-Cr1 (Å)	2.614(9)	2.626(2)	2.616(2)
Cr1-Cr2 (Å)	2.6116(15)	2.625(2)	2.613(2)
Cr2-Cr2 (Å)	2.690(10)	2.706(2)	2.703(2)

The electrical resistivity of $K_2Cr_3As_3$ and $Rb_2Cr_3As_3$ single crystals along the [001] needle direction is presented in Fig. 2, showing T_c values of 6.1 and 4.8 K, respectively, consistent with previous reports [1,2,10]. Transport behavior of $K_2Cr_3As_3$ crystals is quite similar to that previously reported for single-crystal samples [10], showing a marked difference in the temperature dependence as compared to polycrystalline samples that exhibit an anomalous linear temperature dependence above T_c [1–3]. The residual resistivity ratio RRR $= R(300\text{ K})/R(7\text{ K})$ for $K_2Cr_3As_3$ is 15, slightly larger than the reported value of 10 for polycrystals [1,10] and smaller than in previous work [10]. For the latter study, the reported ratio is 50, while the residual resistivity of $\rho_0 \simeq 25\ \mu\Omega\,\text{cm}$ is about half of the value measured in this study, indicating a notable sample dependence of resistivity without a notable change in T_c. For single-crystal $Rb_2Cr_3As_3$ synthesized in the exact same manner as $K_2Cr_3As_3$, we obtain a much larger RRR value of 125 as compared to $K_2Cr_3As_3$ [1,10] and $Rb_2Cr_3As_3$ [2] studies, likely indicating very high crystalline purity in this system and a possible sensitivity to grain boundary effects as encountered in polycrystalline studies.

Interestingly, the resistivity ($\sim$200 $\mu\Omega\,\text{cm}$) of single-crystal $Rb_2Cr_3As_3$ at 300 K is notably reduced compared to

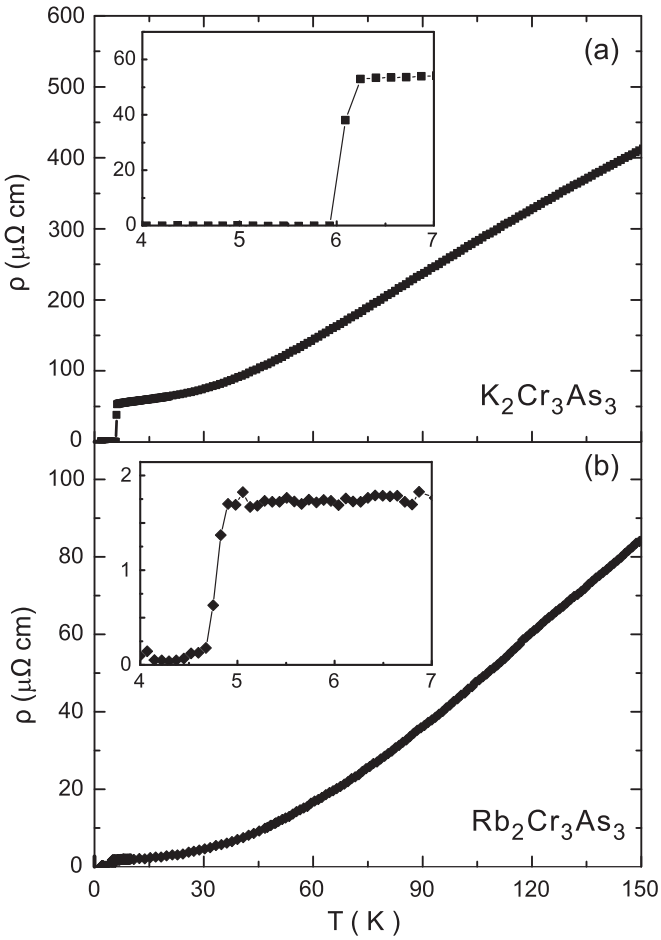

FIG. 2. Resistivity of $K_2Cr_3As_3$ and $Rb_2Cr_3As_3$ single crystals measured along the [001] crystallographic (needle) direction, shown in panels (a) and (b), respectively. Insets present low-temperature zoom, highlighting the superconducting transition in each compound.

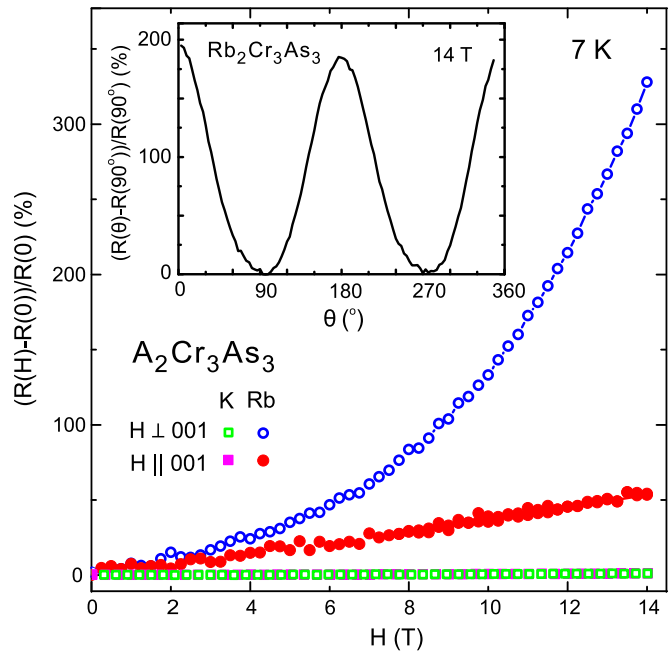

FIG. 3. (Color online) Normalized magnetoresistance of $K_2Cr_3As_3$ and $Rb_2Cr_3As_3$ single-crystal samples measured at 7 K under different field orientation configurations, with current applied along the needle ([001]) direction. The inset presents the field-angle-dependent resistivity of $Rb_2Cr_3As_3$ at 7 K and 14 T.

that of $K_2Cr_3As_3$, by a factor of approximately 4. Assuming the phonon scattering is similar in the two compounds, this decrease may be a result of qualitative changes in the electronic structure, consistent with the theoretical prediction of significant changes in the Fermi surface by J. Wu *et al.* [14], who point out that an extra quasi-1D surface near $[00\pi]$ and changes in the three-dimensional surfaces could result in an increase in conductivity in $Rb_2Cr_3As_3$ as compared to $K_2Cr_3As_3$. We also observe striking contrasts in the magnetoresistance (MR) of $K_2Cr_3As_3$ and $Rb_2Cr_3As_3$ crystals. The extremely small MR measured in $K_2Cr_3As_3$ ($<1\%$ at 7 K and 14 T) is similar to that found in previous work [10], with no measurable difference between the MR measured in both transverse ($H \perp [001]$) and longitudinal $H \parallel [001]$) configurations up to 14 T. This is in stark contrast to the MR of $Rb_2Cr_3As_3$ (Fig. 3), which exhibits a 325% increase in $H \perp [001]$ MR at 7 K and 14 T that is quasiparabolic and linear for $H_\perp$ and $H_\parallel$ orientations, respectively. Moreover, the anisotropy exhibits a twofold symmetry in field-angle rotation measurements shown in Fig. 3, with a 200% change in magnitude between $H_\perp$ and $H_\parallel$ orientations. Considering the similarity of the two systems in all other known properties, this dramatic increase in MR and appearance of strong anisotropy is considered strong evidence for the appearance of quasi-1D components in the electronic structure, consistent with theoretical predictions as noted above [14].

The magnetic susceptibility χ of $K_2Cr_3As_3$ and $Rb_2Cr_3As_3$ single crystals, shown in Fig. 4, confirms the onset of diamagnetic Meissner screening at the same T_c values reported above. In $K_2Cr_3As_3$, a shielding fraction of $\sim 90\%$ is estimated using the zero-field-cooled $\chi(T)$ curve, indicating a significant bulk fraction of superconductivity. In $Rb_2Cr_3As_3$, a smaller apparent fraction of $\sim 30\%$ may be due to difficulties in measuring the much smaller crystals, with needle diameters of 30 μm as compared to 80 μm for $K_2Cr_3As_3$ crystals, and/or due to greater errors in mass determination because of the much more reactive nature of the compound. The isothermal magnetization M was measured for both systems at 1.8 K, as shown in the insets of Fig. 4. The low-field behavior exhibits the characteristic curve of type II superconductors, where H_{c1} can be obtained from the deviation point of the linear field dependence of the $M(H)$ curve, yielding ($H \parallel [001]$) values of 9 and 6 mT in $K_2Cr_3As_3$ and $Rb_2Cr_3As_3$, respectively.

Bulk superconductivity in $Rb_2Cr_3As_3$ is also confirmed by heat capacity measurements on a collection of single crystals (total mass ~ 0.2 mg) oriented with $H \perp [001]$, showing a clear jump in specific heat C at T_c as shown in Fig. 5. The jump is found to decrease in temperature as the magnetic field is increased, indicating the suppression of a bulk superconducting phase transition with field. Values of $T_c(H)$ obtained from the middle point of the jump were plotted in Fig. 7, which shows remarkable consistency with the transport data. Fitting the normal state heat capacity with the expression $C/T = \gamma_n + \beta T^2$, yields values for the electronic Sommerfeld coefficient

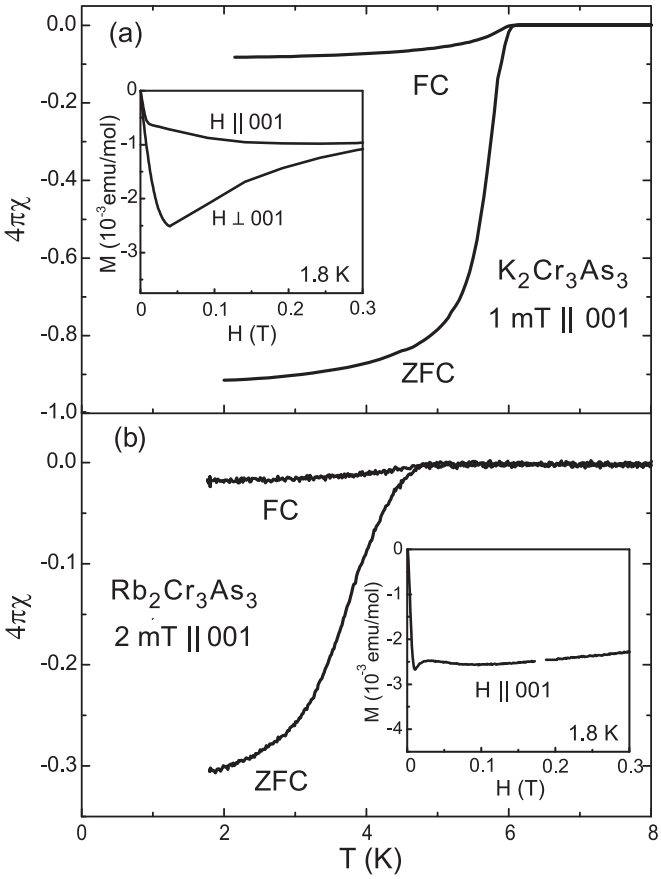

FIG. 4. Magnetic susceptibility of $K_2Cr_3As_3$ and $Rb_2Cr_3As_3$ single-crystal collections under zero-field cooled and field-cooled conditions. Panel (a) presents measurements of $K_2Cr_3As_3$ single crystals with 1 mT field applied along the [001] needle direction. The inset shows field-dependent magnetization of $K_2Cr_3As_3$ single crystals with field applied both parallel and perpendicular to [001]. Panel (b) presents measurements of $Rb_2Cr_3As_3$ single crystals with 2 mT field applied along the [001] needle direction. The inset shows the field-dependent magnetization for parallel ($H_{\parallel}$) fields.

$\gamma_n = 39.5\,\mathrm{mJ\,K^{-2}\,mol^{-1}}$ and the phonon coefficient $\beta = 2.8$ mJ $\mathrm{K^{-4}\,mol^{-1}}$. The value for γ_n is somewhat smaller than that reported for polycrystalline samples (55.1 mJ $\mathrm{K^{-2}\,mol^{-1}}$) [2], while that of β is close to previous reports. We extract the electronic component C_e using these parameters and plot its temperature dependence as $C_e/(\gamma_n T)$ in the inset of Fig. 5, showing the dimensionless heat capacity jump at T_c to be $\Delta C/\gamma_n T_c = 0.62$, much lower than the reported values of 1.8 in $Rb_2Cr_3As_3$ [2] and 2.0–2.4 in $K_2Cr_3As_3$ [1,10]). It is also lower than the BCS value of 1.43 expected for a conventional superconductor, which could be related to the apparent reduced superconducting volume fraction observed in susceptibility measurements noted above, or more intrinsic origins to do with the nature of superconductivity that require further investigation at lower temperatures.

In order to understand the extent of the influence of quasi-1D band structure components on the superconducting state, the anisotropy of H_{c2} was investigated in both $K_2Cr_3As_3$ and $Rb_2Cr_3As_3$. The resistive transition was tracked as a function of field angle, as shown in Figs. 6 and 7, using orientation

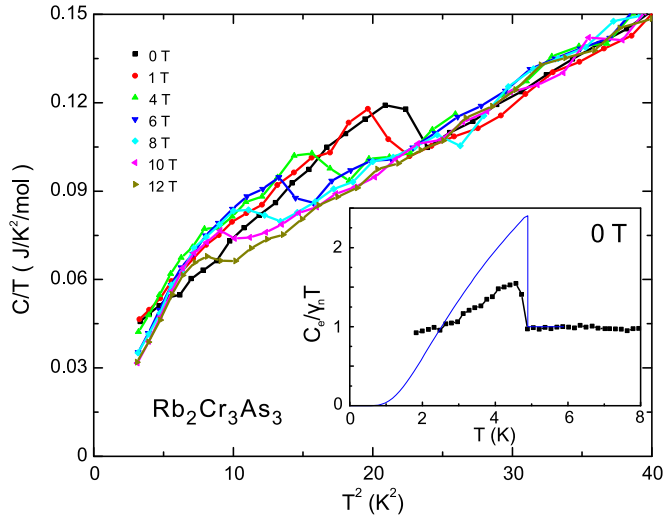

FIG. 5. (Color online) Heat capacity of $Rb_2Cr_3As_3$ single crystals with $H \perp [001]$. The inset shows the normalized electronic specific heat $C_e/(\gamma_n T)$ as a function of temperature; the blue line is the theoretical BCS expectation for a single-band s-wave superconductor (see text).

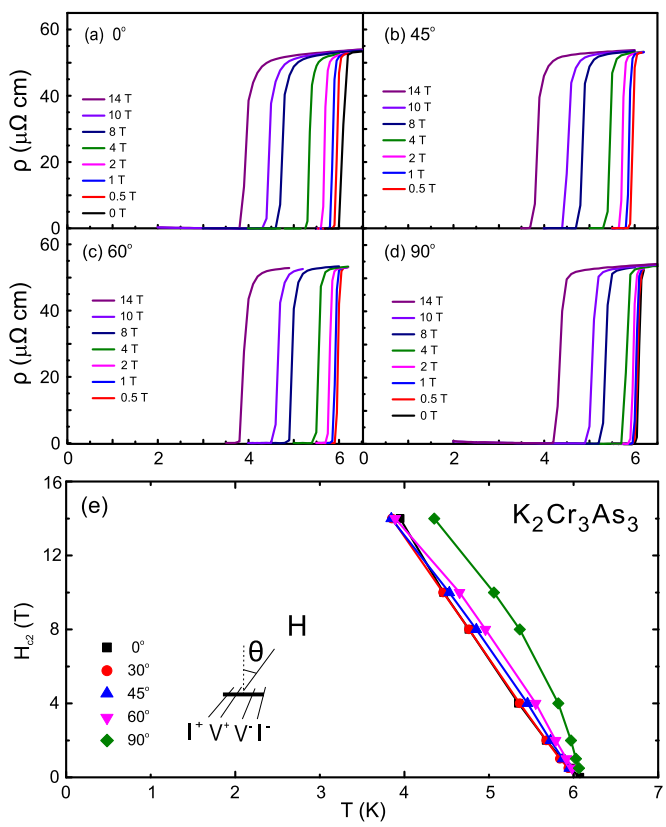

FIG. 6. (Color online) Upper critical field of $K_2Cr_3As_3$ single crystal under different field configurations. Panels (a), (b), (c) and (d) present the field evolution of temperature-dependent resistivity under different field orientations with $\theta = 0°, 45°, 60^o$ and $90°$, respectively. Panel (e) shows the upper critical field temperature dependence in different field orientations as extracted from resistivity transitions in panels (a)–(d), with $T_c(H)$ defined by the midpoint between zero and full resistance.

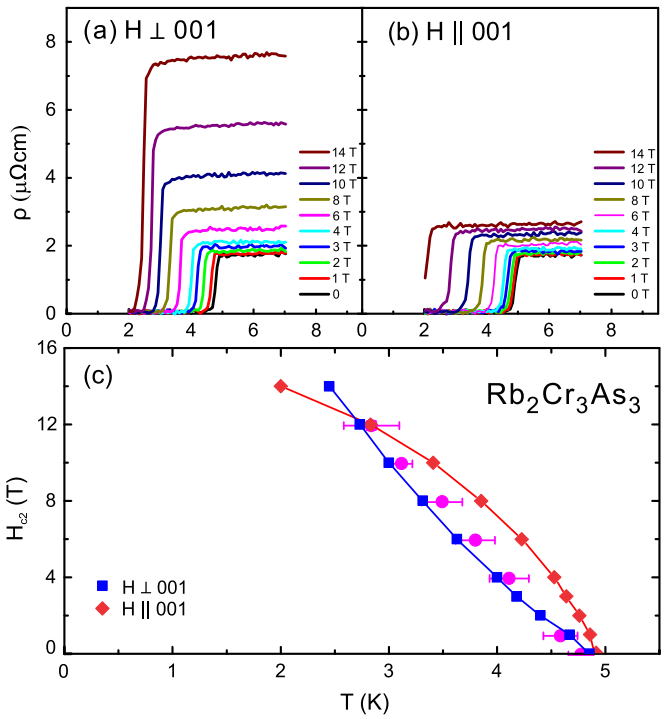

FIG. 7. (Color online) Upper critical field of $Rb_2Cr_3As_3$ single crystal under perpendicular [panel (a)] and parallel [panel (b)] field orientations. Temperature dependence of H_{c2} from resistance data is shown in panel (c), with $T_c(H)$ defined by the midpoint between zero and full resistance. This is compared with T_c (H) data obtained from heat capacity with $H \perp [001]$ orientation (solid purple circles), with T_c values defined by the midpoint of the jump in specific heat and error bars corresponding to the transition width.

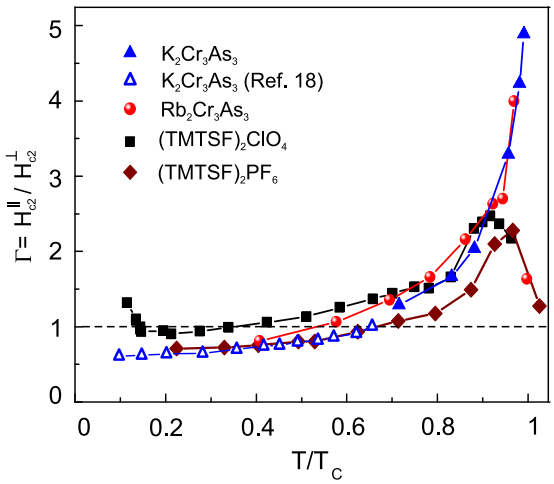

FIG. 8. (Color online) Anisotropy of the upper critical field $\Gamma \equiv H_{c2}^{\parallel}$ (H $\parallel$ 001 for 233, $H \parallel a$ for TMTSF salts)/$H_{c2}^{\perp}$ (H $\perp$ 001 for 233, H $\parallel b$ for TMTSF salts). T_c of $K_2Cr_3As_3$ and $Rb_2Cr_3As_3$ are defined using the midpoint between zero and full resistance. The data for TMTSF salt is taken from Refs. [15] and [5], and high-field data for $K_2Cr_3As_3$ is from Ref. [17].

angles $\theta = 0°$, 45°, 60°, and 90° from the $H_\perp$ orientation for $K_2Cr_3As_3$ and $\theta = 0°$ and 90° for $Rb_2Cr_3As_3$. For $K_2Cr_3As_3$, the initial slope $dH_{c2}(T_c)/dT$ varies from 5.0 to 16.1 T/K, as observed previously [10], with a rapid increase that is even more significant than what were observed in other quasi-1D superconducting states, as shown in Fig. 8. For $Rb_2Cr_3As_3$, the initial slope $dH_{c2}(T_c)/dT$ has a similar range between $H_\perp$ and $H_\parallel$ orientations, with values of 4.4 and 14 T/K, respectively. However, the temperature dependence of $H_{c2}(T)$ in $Rb_2Cr_3As_3$ is quite different than that of $K_2Cr_3As_3$ in the field range up to 14 T, showing a positive curvature for $H_\perp$ and negative curvature for $H_\parallel$ as shown in Fig. 7. In fact, the $H_{c2}(T)$ curves for the two field orientations cross near ~12 T, in a manner similar to that observed in other classic quasi-1D superconductors such as $(TMTSF)_2ClO_4$ [15] and $(TMTSF)_2PF_6$ [5]. In these organic superconductors, a similar trend is observed where a diverging temperature dependence is observed in the $H_\perp$ orientation, while a saturating Pauli-limited dependence occurs for $H_\parallel$ (parallel to the conducting direction). In Li-based purple bronze, such Pauli-limited behavior can be also observed with fields applied along the conducting chain, while a divergent behavior is observed in the other two field orientations [16].

Recent pulsed-field work on $K_2Cr_3As_3$ single crystals indeed shows such a crossing to occur at higher fields, with $H_{c2}^{\perp}(T)$ surpassing $H_{c2}^{\parallel}(T)$ near 15 T and indications of Pauli-limited behavior in the $H_\parallel$ orientation [17]. Figure 8 presents a comparison between the $A_2Cr_3As_3$ compounds and the organic systems $(TMTSF)_2ClO_4$ and $(TMTSF)_2PF_6$, plotting the temperature dependence of the H_{c2} anisotropy parameter $\Gamma(T) = H_{c2}^{\parallel}(T)/H_{c2}^{\perp}(T)$ (with $H_\parallel$ and $H_\perp$ relative to the c axis for $A_2Cr_3As_3$, and in the a- and c-axis directions, respectively, for TMTSF salts). A similar change in Γ, from large near T_c to near unity at lower temperatures, is seen in both the organics and $A_2Cr_3As_3$ materials, indicating a resemblance. Although a similar $\Gamma(T)$ evolution was also found in higher-dimensional systems such as K-doped $BaFe_2As_2$ [18,19], the notable difference is in the crossing (i.e., $\Gamma = 1$) point, where the $H_\perp$ component begins to take off in the quasi-1D systems. While a mild anisotropy was previously reported for $K_2Cr_3As_3$ single crystals [10], it is clear that the observable trend in the limited field range available for our measurements of $K_2Cr_3As_3$ is very similar to that of $Rb_2Cr_3As_3$, and indeed follows the same behavior at higher fields [17] as shown in Fig. 8 for a normalized temperature regime.

Although higher field data for $Rb_2Cr_3As_3$ is lacking, the apparent likeness of $\Gamma(T)$ between $Rb_2Cr_3As_3$ and $K_2Cr_3As_3$ presents an apparent contradiction: contrasting MR anisotropies are suggestive of a highly tunable quasi-1D normal state electronic structure that differs in the two compounds, while the normalized $\Gamma(T)$ behavior is very comparable for each. This conundrum could be readily dismissed if Pauli limiting were the dominant pair-breaking mechanism, as the comparison of superconducting condensation energy and Zeeman energy is, to first order, independent of details of the electronic band structure of the host material. However, the observed combination of orbital ($H_\perp$) and Pauli ($H_\parallel$) limited H_{c2} behaviors in $K_2Cr_3As_3$ [17] calls for a less simplified explanation. For instance, the spin-locked Cooper pairing scenario proposed by Balakirev *et al.*, where the pair singlet

spins are pinned along the quasi-1D chain direction [17], may provide a pair-breaking scenario common to all $A_2Cr_3As_3$ superconductors, given their pairing attraction is indeed tied to a low-dimensional spin fluctuation mechanism in all three systems. Above all, this highlights the need for detailed experimental studies of the electronic structure as well as higher-field H_{c2} studies of $Rb_2Cr_3As_3$ in order to understand how the anisotropy of superconducting state properties is affected by the strongly enhanced normal state anisotropy found in $Rb_2Cr_3As_3$.

In summary, we report successful synthesis of high-quality $A_2Cr_3As_3$ single crystals with $A = K$ and Rb using a self-flux method, providing the first comparison of single-crystal properties between two members of this new superconductor family. The increase in ionic size from K to Rb causes an increase in the spacing between quasi-one-dimensional chains in the hexagonal crystal structure of $Rb_2Cr_3As_3$ as compared to $K_2Cr_3As_3$, while keeping the intrachain dimensions mostly unchanged. While the superconducting state properties are comparable between the two systems, the normal state resistivity shows a striking evolution, with a 325% enhancement of magnetoresistance and the appearance of strong anisotropy in $Rb_2Cr_3As_3$. These properties point to a strong quasi-one-dimensional component in the electronic properties that evolves with enhanced unit cell dimensions in the $A_2Cr_3As_3$ system. The similarities to other well-established quasi-1D superconductors deserves further attention.

The authors acknowledge R. L. Greene, H. Hodovanets, J. P. Hu, Y. P. Jiang, L. M. Wang, and X. H. Zhang for valuable discussions and experimental assistance. This work was supported by AFOSR through Grant No. FA9550-14-1-0332 and the Gordon and Betty Moore Foundation's EPiQS Initiative through Grant No. GBMF4419.

[1] J.-K. Bao, J.-Y. Liu, C.-W. Ma, Z.-H. Meng, Z.-T. Tang, Y.-L. Sun, H.-F. Zhai, H. Jiang, H. Bai, C.-M. Feng, Z.-A. Xu, and G.-H. Cao, Superconductivity in quasi-one-dimensional $K_2Cr_3As_3$ with significant electron correlations, Phys. Rev. X **5**, 011013 (2015).

[2] Z. T. Tang, J. K. Bao, Y. Liu, Y. L. Sun, A. Ablimit, H. F. Zhai, H. Jiang, C. M. Feng, Z. A. Xu, and G. H. Cao, Unconventional superconductivity in quasi-one-dimensional $Rb_2Cr_3As_3$, Phys. Rev. B **91**, 020506(R) (2015).

[3] Z. T. Tang, J. K. Bao, Z. Wang, H. Bai, H. Jiang, Y. Liu, H. F. Zhai, C. M. Feng, Z. A. Xu, and G. H. Cao, Superconductivity in quasi-one-dimensional $Cs_2Cr_3As_3$ with large interchain distance, Sci. China Mater. **58**, 16 (2015).

[4] J. Shinagawa, Y. Kurosaki, F. Zhang, C. Parker, S. E. Brown, D. Jérome, J. B. Christensen, and K. Bechgaard, Superconducting state of the organic conductor $(TMTSF)_2ClO_4$, Phys. Rev. Lett. **98**, 147002 (2007).

[5] I. J. Lee, M. J. Naughton, G. M. Danner, and P. M. Chaikin, Anisotropy of the upper critical field in $(TMTSF)_2PF_6$, Phys. Rev. Lett. **78**, 3555 (1997).

[6] D. Jerome, A. Mazaud, M. Ribault, and K. Bechgaard, Superconductivity in a synthetic organic conductor $(TMTSF)_2PF_6$, J. Phys. Lett. **41**, 95 (1980).

[7] K. Bechgaard, K. Carneiro, M. Olsen, F. B. Rasmussen, and C. S. Jacobsen, Zero-pressure organic superconductor: Di-(Tetramethyltetraselenafulvalenium)-Perchlorate $[(TMTSF)_2ClO_4]$, Phys. Rev. Lett. **46**, 852 (1981).

[8] M. Greenblatt, W. H. McCarroll, R. Neifeld, M. Croft, and J. V. Waszczak, Quasi two-dimensional electronic properties of the lithium molybdenum bronze, $Li_{0.9}Mo_6O_{17}$, Solid State Commun. **51**, 671 (1984).

[9] J. C. Armici, M. Decroux, O. Fischer, M. Potel, R. Chevrel, and M. Sergent, A new pseudo-one-dimensional superconductor: $Tl_2Mo_6Se_6$, Solid State Commun. **33**, 607 (1980).

[10] T. Kong, S. L. Bud'ko, and P. C. Canfield, Anisotropic H_{c2}, thermodynamic and transport measurements, and pressure dependence of T_c in $K_2Cr_3As_3$ single crystals, Phys. Rev. B **91**, 020507(R) (2015).

[11] G. M. Pang, M. Smidman, W. B. Jiang, J. K. Bao, Z. F. Weng, Y. F. Wang, L. Jiao, J. L. Zhang, G. H. Cao, and H. Q. Yuan, Evidence for nodal superconductivity in quasi-one-dimensional $K_2Cr_3As_3$, Phys. Rev. B **91**, 220502(R) (2015).

[12] H. Z. Zhi, T. Imai, F. L. Ning, J. K. Bao, and G. H. Cao, NMR Investigation of the quasi-one-dimensional superconductor $K_2Cr_3As_3$, Phys. Rev. Lett. **114**, 147004 (2015).

[13] K. Kihou, T. Saito, S. Ishida, M. Nakajima, Y. H. Fukazawa, Y. Kohori, T. Ito, S. Uchida, A. Iyo, C. Lee, and H. Eisaki, Single crystal growth and characterization of the iron-based superconductor KFe_2As_2 synthesized by KAs flux method, J. Phys. Soc. Jpn. **79**, 124713 (2010).

[14] X. X. Wu, C. C. Le, J. Yuan, H. Fan, and J. P. Hu, Magnetism in quasi-one-dimensional $A_2Cr_3As_3$ (A=K,Rb) superconductors, Chinese Phys. Lett. **32**, 057401 (2015).

[15] S. Yonezawa, S. Kusaba, Y. Maeno, P. Auban-Senzier, C. Pasquier, K. Bechgaard, and D. Jérome, Anomalous in-plane anisotropy of the onset of superconductivity in $(TMTSF)_2ClO_4$, Phys. Rev. Lett. **100**, 117002 (2008).

[16] J.-F. Mercure, A. F. Bangura, X. Xu, N. Wakeham, A. Carrington, P. Walmsley, M. Greenblatt, and N. E. Hussey, Upper critical magnetic field far above the paramagnetic pair-breaking limit of superconducting one-dimensional $Li_{0.9}Mo_6O_{17}$ single crystals, Phys. Rev. Lett. **108**, 187003 (2012).

[17] F. F. Balakirev, T. Kong, M. Jaime, R. D. McDonald, C. H. Mielke, A. Gurevich, P. C. Canfield, and S. L. Bud'ko, Anisotropy reversal of the upper critical field at low temperatures and spin-locked superconductivity in $K_2Cr_3As_3$, Phys. Rev. B **91**, 220505(R) (2015).

[18] M. M. Altarawneh, K. Collar, C. H. Mielke, N. Ni, S. L. Bud'ko, and P. C. Canfield, Determination of anisotropic H_{c2} up to 60 T in $Ba_{0.55}K_{0.45}Fe_2As_2$ single crystals, Phys. Rev. B **78**, 220505 (2008).

[19] H. Q. Yuan, J. Singleton, F. F. Balakirev, S. A. Baily, G. F. Chen, J. L. Luo, and N. L. Wang, Nearly isotropic superconductivity in $(Ba,K)Fe_2As_2$, Nature (London) **457**, 565 (2009).